Simulation of nanodiamond and nanographite formation from molten carbon in the presence of hydrogen

A. Sorkin, Joan Adler,* and R. Kalish
Department of Physics, Technion, Israel Institute of Technology, Haifa 32000, Israel
(Received 11 February 2008; published 29 October 2008)

Hydrogen plays a significant role in the formation of nanodiamond, terminating diamond surfaces, and removing sp^2-bonded atoms from the surface during chemical-vapor deposition diamond growth. However, there are only few calculations that simulate nanodiamond development directly and even less that do so in a hydrogen-containing environment. Recently, nanoscale graphitic layers embedded in amorphous carbon were observed experimentally. We report here on results from a comprehensive study of nanodiamond and nanographite formation from molten carbon in the presence of hydrogen under varied conditions of external pressure and cooling rate. We find that hydrogen-free nanodiamond crystals are precipitated more readily at increased melt densities and cooling rates, whereas slower cooling rates permit formation of graphitic layers.

DOI: 10.1103/PhysRevB.78.155435 PACS number(s): 62.50.−p, 81.05.Uw, 61.43.Bn

I. INTRODUCTION

A carbon atom can bond to another C atom with different bonding configurations including sp^2, which is the bonding in graphite and sp^3, as what occurs in diamond.[1] Carbon can also form amorphous structures (denoted by a-C), in which the bonding can be predominantly sp^2 (graphitelike), sp^3 (diamondlike), or a mixture of both. The extremely different physical and chemical properties of diamond and graphite are also reflected in their amorphous forms. Diamondlike amorphous carbon (DLC) in which the C atoms are predominantly tetrahedrally (sp^3) bonded is denoted as ta-C and possesses many of the very attractive properties of diamond. Therefore it is a material of great technological importance.

Hydrogen readily bonds to C, giving rise to an enormous variety of molecules which are the building blocks of organic chemistry. When hydrogen is present in the various forms of amorphous carbon, it forms amorphous hydrogenated carbon, which is denoted by a-C:H. The properties of a-C and a-C:H materials, theories of formation and structure as well as their production, have recently been reviewed by Robertson.[2]

Hydrogen can also be present in crystalline diamond, occupying interstitial positions—the locations of which are still under dispute.[3] Hydrogen on a diamond surface gives rise to a negative electron affinity and other interesting properties.[4] The presence of hydrogen could reduce the gap in the density of states in amorphous diamond.[5] Hydrogen is an essential ingredient for the growth of diamond by chemical-vapor deposition (CVD) methods, as the abundant (usually more than 95%) presence of hydrogen in the C-containing growth plasma is necessary for the growth of high-quality diamond. It is believed that the role of (atomic) hydrogen during CVD diamond growth is to remove undesired sp^2 bonded atoms from the growth surface and assist the crystal formation by saturating the dangling C surface bonds.

An interesting question, which is addressed here, is whether the presence of hydrogen in molten amorphous carbon also assists the formation of diamond crystallites during the cooling of the liquid. In other words, would a material that might solidify as hydrogen-containing tetrahedral carbon also contain some diamond crystallites? The subnanodiamond grains may serve as nucleation centers for further diamond growth as predicted and described by the subimplantation model of Lifshitz *et al.*[6,7] This model was developed for hydrogen-free amorphous carbon layers formed during high-dose low-energy C ion implantation. Michaelson and Hoffman[8] provided experimental evidence for this mechanistic model.

In this paper, we describe our studies of the structural and electronic properties of hydrogenated amorphous carbon networks generated with different densities and cooling rates, and with different contents of hydrogen atoms with tight-binding molecular-dynamics (MD) simulations. We found that hydrogen-free nanodiamond crystals were formed within the compressed hydrogenated amorphous matrix; the hydrogen atoms are being expelled from these diamond clusters. The probability of precipitation of diamond clusters increases with increasing density and cooling rates, and slightly decreases with hydrogen content. The orientations of the diamond clusters were found to be random. The possibility of transforming amorphous carbon into oriented graphitic planes has recently been described.[9] For slower cooling rates we indeed observed such layers in visualizations of our simulated samples under certain conditions.

II. COMPUTATIONAL INTRODUCTION

Many authors have simulated the structure of pure or hydrogenated amorphous carbon networks that were generated under conditions close to those occurring within the "thermal spike."[6,10–16] Most of these, except for Refs. 15 and 16, did not involve external pressure. Only a few observed a nucleation of diamond. For example, Kopidakis *et al.*[10] investigated the structures of hydrogenated amorphous carbon networks by orthogonal tight-binding molecular-dynamics simulations. They found that hydrogen tends to break carbon-carbon bonds in tetrahedral amorphous carbon, ta-C. This reduction in C-C coordination makes ta-C softer and induces more electronic states in the energy-band gap region. As can be seen from our description below the conditions of their simulations were very similar to those reported in our

study. However, in contrast to our findings, which clearly show nanodiamonds embedded in the amorphous matrix, the authors of Ref. 10 did not identify any ordered sp^3 clusters in their samples.

Ofer *et al.*[11] simulated a hydrogenated amorphous carbon-diamond composite with a tight-binding method. They found that the total fraction of sp^3-bonded carbon atoms was not a monotonic function of hydrogen concentration. As the number of H atoms increases, the number of sp^3 bonds also increases until the saturation of H was achieved and a decrease in the number of sp^3 bonds began. In their visualizations one can see that the new sp^3 bonds form near previously formed sp^3 bonds, which suggest growth of a diamond cluster.

Kohary *et al.*[12] simulated the ion bombardment process during bias-enhanced nucleation (BEN) by the nonorthogonal tight-binding method. A heated a-C:H layer was bombarded with methyl and acetylene ions of different energies. The bombardment caused structural rearrangement in the substrate resulting in an increase in the total sp^3 content in the film, while the total sp^2 content is decreased by the same magnitude. No formation of diamond nuclei or aligned graphitic planes was observed. The nonorthogonal tight-binding simulations of the first stage of diamond nucleation process in a dense amorphous hydrogenated carbon that was carried out by Lifshitz *et al.*[6] showed that a diamondlike sp^3 cluster could spontaneously form in a hydrogenated amorphous carbon network (25% of hydrogen atoms) generated at a density of 3 g/cc. The hydrogen was concentrated in the more porous parts of the cell and decorated the surface of the sp^3 clusters, mainly forming sp^3 C-H bonds.

In a previous paper[15] we studied the nucleation of diamond from liquid carbon without hydrogen under extreme pressures. We observed the formation of large diamond crystallites in an amorphous carbon network generated at densities of 3.5–3.9 g/cc and fast cooling rates (1000 K/ps). We found that the probability of precipitation of diamond crystallites increases with density and with cooling rate. At slower cooling rates (200–500 K/ps), some samples transformed to graphite.

The conditions of the Ref. 15 simulations, which describe solidification of hydrogen-free liquid C, are very similar to those of Wang *et al.*,[16] who investigated the structure of amorphous carbon over a wide range of densities (from 2.2 to 4.4 g/cc) that are generated by rapid quenching of liquid carbon phase by the same method. The authors did not identify any ordered sp^3 clusters in their samples. We note two reasons for this discrepancy: first, the precipitation of diamond clusters is a random process, and if the number of realizations is small, the probability of generating an amorphous carbon sample with a crystalline diamond cluster within is not large. The statistics of Wang *et al.*[16] could be insufficient to identify large diamond crystallites in their samples. The second reason is that it is difficult to identify a small diamond crystallite in a large amorphous sp^3-bonded carbon network without modern visualization tools. One such tool is our atomic visualization (AViz) (Ref. 17) package which possesses all the capabilities needed to identify diamond clusters.

Fast quenching of a compressed hydrogenated liquid carbon sample, similar to that occurring during the BEN process, is possibly the laboratory system closest to our simulations. The times available to perform MD computations (a few picoseconds) and the sample sizes (containing a few hundred atoms) are similar to those of the thermal spike. The densities at which our simulations were carried out (3.5 and 3.9 g/cc) can reasonably be locally attained within the thermal spike. The hydrogen content in our samples does not exceed 10%, while the optimal hydrogen concentration for diamond nucleation in an a-C:H matrix during BEN is 25%.[6] The reason for such a low hydrogen content in our calculations is that no liquid carbon with a high hydrogen content could be obtained perhaps because the velocities of the moving hydrogen atoms are so much higher than those of carbon atoms. The temperatures required in order to melt carbon are 6000–8000 K. At these temperatures the velocity of hydrogen atoms is so high that our tight-binding code is capable of only treating a few hydrogen atoms without collapse of the sample.

Because of the low probability of nucleationlike phenomena, relatively long simulations of relatively large systems are needed. Such simulations are not realistic with *ab initio* methods. In this respect, tight-binding simulations, such as ours, are a reasonable compromise between accurate but slow *ab initio* calculations and calculations with empirical potentials, which are fast but do not ensure sufficient accuracy. Reliability of tight-binding molecular dynamics[16,18] as well as the effects of small sample sizes were discussed by us previously.[15]

III. DETAILS OF THE SIMULATIONS

Our calculations were carried out at constant volume (density). Periodic boundary conditions were applied to the samples in all three directions. In order to describe the interactions between carbon atoms we used the tight-binding model[18] of the OXON package.[19] The electron wave functions were expanded in terms of a basis set of valence electron wave functions, controlling the attractive part of the potential, while the repulsive one was treated empirically. The Γ-point Brillouin-zone sampling was used for the electronic calculations and the MD step was 1×10^{-15} s. Visualization with AViz (Ref. 17) was applied to identify diamond clusters as mentioned above.

The samples used in the simulations were initially arranged as a perfect diamond crystal of a size $3\times3\times3$ unit cells (i.e., 216 carbon atoms) with a density of 3.5 g/cc (i.e.,

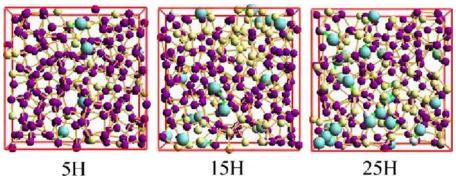

FIG. 1. (Color online) A-C:H structures with different content of hydrogen atoms. The black, gray, and white balls (purple, yellow, and white online) are the carbon atoms with four, three, and two C-C bonds (excluding C-H bonds), respectively. Hydrogen atoms are represented by large gray (light blue online) balls.

TABLE I. Average number (rounded to nearest integer) of differently bonded carbon atoms in the a-C:H samples generated at 3.9 g/cc and with a cooling rate of 1000 K/ps.

Number of H atoms in the a-C:H sample	0	5	10	15	25
Number of C atoms with four C-C and zero C-H bonds	190	186	172	150	151
Number of C atoms with three C-C and zero C-H bonds	24	22	32	47	31
Number of C atoms with two C-C and zero C-H bonds	2	3	2	4	5
Number of C atoms with four C-C and one C-H bonds	0	0	0	0	2
Number of C atoms with three C-C and one C-H bonds	0	5	9	13	21
Number of C atoms with three C-C and two C-H bonds	0	0	0	0	1
Number of C atoms with two C-C and one C-H bonds	0	0	1	2	4
Number of C atoms with two C-C and two C-H bonds	0	0	0	0	1
Total number of sp^3-bonded C atoms	190	191	181	163	172
Total number of sp^2-bonded C atoms	24	22	33	49	35
Total number of sp-bonded C atoms	2	3	2	4	5

the sides of simulation box were 10.65 Å). The diamond was melted at a temperature of 8000 K during 5, 10, 15, 20, and 25 ps. These five liquid carbon samples were rapidly cooled with a cooling rate of 500 K/ps. In order to generate samples of amorphous carbon with a higher density, each of the configurations was isotropically compressed by changing the volume of the unit cell to the densities of 3.9 g/cc (the length of simulation box was decreased up to 10.3 Å). We then placed 5–25 hydrogen atoms in each sample at both densities (3.5 and 3.9 g/cc). Pairs of neighboring bonded carbon atoms were randomly chosen, and the hydrogen atoms were positioned at the midpoint of the bond between them. The volume of the simulation box remained unchanged; hence, the resulting density of the sample slightly increases as the number of H atoms increases. Then the hydrogenated samples were repeatedly heated up to 6000 K and cooled to room temperature with three different cooling rates: fast (1000 K/ps), intermediate (500 K/ps), and slow (200 K/ps). In total, 120 simulations were carried out.

The entire computational effort of all the calculations for the many different cases, careful sample preparations, adequate statistics, and equilibration was substantial. Several fast Pentium workstations, each with several gigabyte of random access memory (RAM), were used for more than one year. We have found OXON (Ref. 19) to be a very helpful tool for efficient tight-binding simulations, but even for our sample sizes the computations were memory limited as well as being time limited. For the present project the sample sizes and boundary conditions used are indeed adequate for the thermal spike type of phenomena that we are researching here. This would, however, not be the case if we were to concern ourselves with interfaces between distinct carbon allotropes.

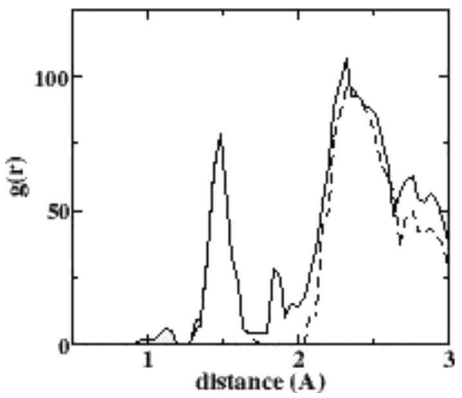

FIG. 2. Radial distribution function of the hydrogenated amorphous carbons containing 25 hydrogen atoms generated at 3.9 g/cc with the intermediate cooling rate (solid line) compared with that for C-C bonds only (dashed line). Additional peaks of the complete radial distribution located at ~1.13 and ~1.86 Å represent the distances from H atoms to nearest and second-nearest carbon atoms, respectively.

IV. RESULTS

A. Structure of hydrogenated amorphous carbon

Typical structures of the a-C:H samples generated at the initial density of 3.9 g/cc with the fast cooling rate (1000 K/ps) and with different content of hydrogen atoms are presented in Fig. 1. Averages of the detailed counts of differently bonded atoms as a function of hydrogen concentration

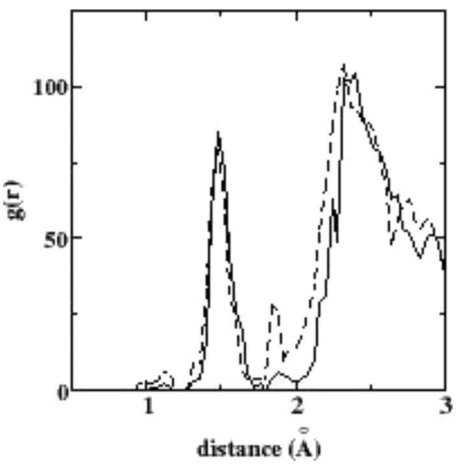

FIG. 3. Radial distribution function of the hydrogenated amorphous carbon samples generated at 3.9 g/cc containing 5 hydrogen atoms (solid line) and containing 25 hydrogen atoms (dashed line).

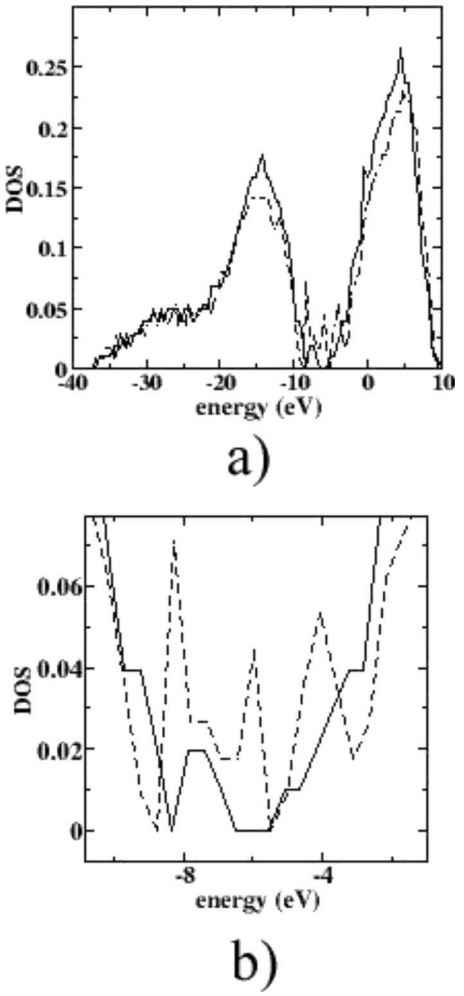

FIG. 4. (a) Density of states of the hydrogenated amorphous carbon samples at 3.9 g/cc, containing 5 hydrogen atoms (solid line) and 25 hydrogen atoms (dashed line). In (b) a magnified part of the density of states near the band gap is shown.

in these samples are listed in Table I. It is clearly seen that the increase in hydrogen atom content systematically reduces the number of sp^3-bonded carbon atoms with four carbon neighbors.

For example, in the samples with five hydrogen atoms there are, on average, 186 fourfold carbon atoms with four carbon neighbors, while in the sample with 15–25 hydrogen atoms there are 150–151 such atoms. At the same time the average number of carbon atoms with three carbon neighbors and a single hydrogen neighbor increases from 5 to 21 as the number of hydrogen atoms is increased from 5 to 25. It is clear that the hydrogen atoms break the C-C bonds and replace carbon atoms. The total fraction of sp^3-bonded atoms (C atoms with four C-C bonds, C atoms with three C-C and one C-H bonds, and C atoms with two C-C and two C-H bonds) appears to decrease with hydrogen concentration within our accuracy for this case of initial density (3.9 g/cc) and fast cooling rate. Only a few fivefold carbon (C with four C-C and one C-H bonds, and C with three C-C and two C-H bonds) atoms were found, appearing only in the samples with 25 hydrogen atoms. (The slight nonmonotonicities are probably indicative of our statistical errors, but we cannot exclude a connection with the fivefold atoms for the case with the highest number of hydrogen atoms.)

TABLE II. Band gap of the samples prepared at 3.9 g/cc with the fast cooling rate.

Number of H atoms	sp^3 fraction (%)	Band gap (eV)
0	82–90	1.3–3.7
5	80–88	0.3–1
10	80–85	0

The radial distribution function of the sample containing 25 hydrogen atoms is shown in Fig. 2. On the same figure we draw the partial radial distribution function of C-C bonds only. The complete radial distribution function has two low additional peaks located at ~1.13 and ~1.86 Å, which are the distances from H atoms to the nearest and next-nearest carbon atoms, respectively. The high peaks located at 1.52 and 2.4 Å represent the nearest carbon neighbors and next-nearest carbon neighbors for carbon atoms. We did not find any detectable dependence of C-C and C-H bond lengths on the number of hydrogen atoms in the samples within our range of hydrogen content. The average C-C and average C-H bond lengths were equal for all hydrogenated amorphous carbon samples generated at 3.9 g/cc and at the fast cooling rate (1.13 Å). This can be observed in Fig. 3, where the radial distribution functions of the hydrogenated amorphous carbon containing 5 and 25 hydrogen atoms are presented.

TABLE III. Number of carbon atoms with four C-C bonds (sp^3) or indication of the formation of nanographitic crystallites in the samples with 0, 5, or 25 hydrogen atoms generated with different densities and different cooling rates.

Number of H atoms	Density (g/cc)	Fast	Intermediate	Slow
0	3.5	73,69,76,74,67	76,77,graphite,66,80	64,66,graphite,graphite,75
0	3.9	89,88,82,90,89,85	89,84,85,89,92	graphite,77,51,74,graphite
5	3.5	68,77,63,71,71	69,68,graphite,61,58	73,74,67,graphite,65
5	3.9	83,80,88,86,86	80,90,77,80,86	78,85,57,88,82
25	3.5	51,54,67,62,57	51,61,61,56,51	67,graphite,49,53,graphite
25	3.9	70,73,67,69,67	71,72,68,69,71	75,71,67,73,70,graphite

TABLE IV. Number of samples where diamond clusters containing more than ten atoms were found from sets of five samples generated at high density (3.9 g/cc).

Number of H atoms	Fast	Intermediate	Slow
0	4	1	1
5	1	2	0
10	1	1	0
15	1	0	1
25	0	2	0

The density of states of the samples generated at 3.9 g/cc with fast cooling rate is shown in Fig. 4 for different numbers of hydrogen atoms. The presence of hydrogen decreases the band gap. For example, without hydrogen, an amorphous carbon sample with 90% of sp^3-coordinated atoms shows a band gap of 3.7 eV, while the band gap of the hydrogenated amorphous carbon with five hydrogen atoms and 86% of sp^3-bonded carbon atoms is 1 eV only. The reduction in the band gap with the increasing content of hydrogen is shown in Table II. The samples with 10–25 hydrogen atoms did not show any band gap.

We explored the influence of different cooling rates and different densities on the structure of the hydrogenated amorphous carbon samples. In Table III we show the fraction of carbon atoms with four C-C bonds (sp^3) in the samples with 5 and 25 hydrogen atoms that are generated with different densities and different cooling rates—each for five different samples. As in the case of amorphous carbon without hydrogen[15] the fraction of sp^3-bonded atoms decreases as the density decreases. A systematic influence of cooling rate on sp^3 content was not found. It should be noted that for intermediate and slow cooling rates some graphitic structures were identified, as will be discussed below.

B. Diamond nucleation in the hydrogenated carbon network

Most of the structures formed were highly inhomogeneous and contained large sp^3 clusters that do not include hydrogen. Hydrogen seems to escape from these pure sp^3 clusters. This sp^3 clustering signifies the initial stage of diamond cluster formation; some of the sp^3 clusters generated within our hydrogenated amorphous carbon samples clearly show a diamond structure. The clusters appeared in at least one case in each row (number of hydrogen atoms) of our summary in Table IV, where we list the number of diamond clusters containing more than ten atoms for samples generated with the initial density of 3.9 g/cc for all cooling rates. From Table IV we conclude that the probability of diamond nucleation at fast and intermediate cooling rates appears to be slightly higher than at slow cooling rate. The dependence of the diamond nucleation on hydrogen content is not completely monotonic. When no hydrogen atoms were inserted, fast cooling rates led to many large clusters at high density. At the low density of 3.5 g/cc we found only two cases where the sp^3 cluster had an ordered diamond structure: in the sample with five hydrogen atoms at intermediate cooling rate and in the sample with ten hydrogen atoms at fast cooling rate.

The best large diamond cluster was found in the sample generated at intermediate (500 K/ps) cooling rate within the sample with ten hydrogen atoms that are generated with high initial density (3.9 g/cc). This diamond cluster, shown in Fig. 5 and viewed from different angles, is free from hydrogen atoms. The orientation of the diamond clusters relative to the walls of the simulation box was found to be arbitrary.

The obtained nanodiamonds were investigated by performing statistical analysis of their radial and angular distribution functions, as shown in Figs. 6 and 7. The first peak of the radial distribution function is located at 1.53 Å, which is very close to that of diamond, 1.54 Å. The peak of the angular distribution function is located at 111°, which is also close to the diamond peak at 109°. The density of states inside this cluster (see Fig. 8) shows a band gap of ~4 eV, which is slightly narrower than the band gap of perfect diamond at 3.5 g/cc with 5.4 eV.

C. Nanographitic crystallites

A number of samples generated at intermediate (500 K/ps) and slow cooling rates (200 K/ps) exhibited clear formation of nanographitic crystallites, one such case is shown in Fig. 9. Note that not all the planes have a perfect graphitic structure. In Table III such graphitic configurations are listed, and we note that they did not form more than twice in each set of five samples. These graphitic configurations appeared more frequently at low density (3.5 g/cc) and for the slowest cooling rates. The orientation of the graphitic planes was random.

The radial distribution function of an entire sample (25 hydrogen atoms generated at 3.9g/cc at a slow cooling rate),

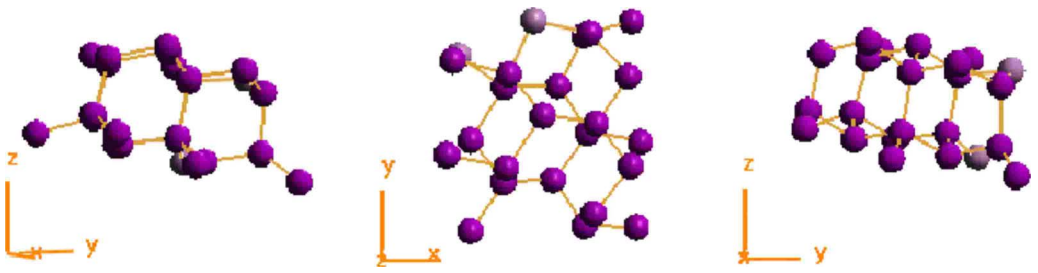

FIG. 5. (Color online) A diamond cluster containing 22 carbon atoms found in the sample with 10 hydrogen atoms that are generated at intermediate cooling rate.

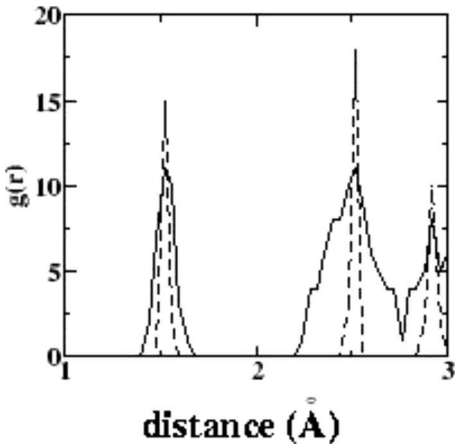

FIG. 6. Radial distribution function of a diamond cluster inside hydrogenated amorphous carbon, containing ten hydrogen atoms generated with intermediate cooling rate (solid line), compared with the radial distribution function of pure diamond (dashed line).

in which graphitic sheets were obtained, is compared with that for C-C bonds only—shown in Fig. 10. The average C-H bond length in the graphitic configurations varied from ~1.02 to ~1.1 Å, as the density decreases from 3.9 to 3.5 g/cc. The interplanar distance is shorter than that of perfect graphite: 2.1 and 2.5 Å for the samples generated at 3.9 and 3.5 g/cc, respectively; however, the present densities are much higher than those of perfect graphite (2.2 g/cc). The peak of the angular distribution function of the graphitic configuration, while broader than that of perfect graphite, is also located around 120° (see Fig. 11) which is the angle between two C atoms in perfect graphite.

V. SUMMARY

We have simulated precipitation of diamond and graphitic crystallites in compressed hydrogenated amorphous carbon samples generated by rapid quenching of liquid carbon. The

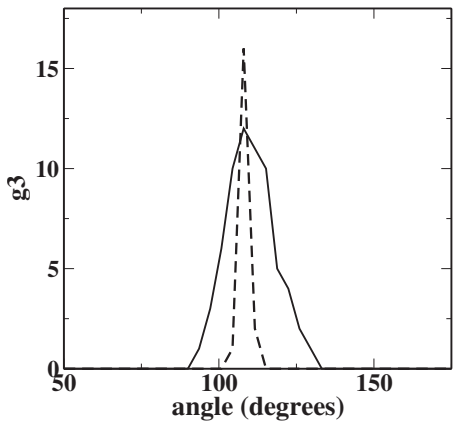

FIG. 7. Angular distribution function of diamond cluster inside hydrogenated amorphous carbon, containing ten hydrogen atoms generated at 3.9 g/cc with fast cooling rate (solid line), compared with the angular distribution function of pure diamond (dashed line).

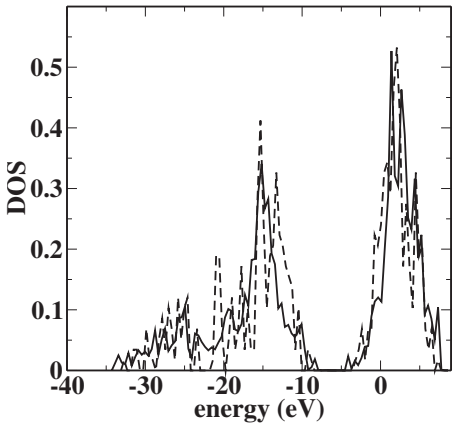

FIG. 8. Density of states of diamond cluster inside hydrogenated amorphous carbon, containing ten hydrogen atoms generated at 3.9 g/cc with intermediate cooling rate (solid line), compared with the density of states of pure diamond (dashed line).

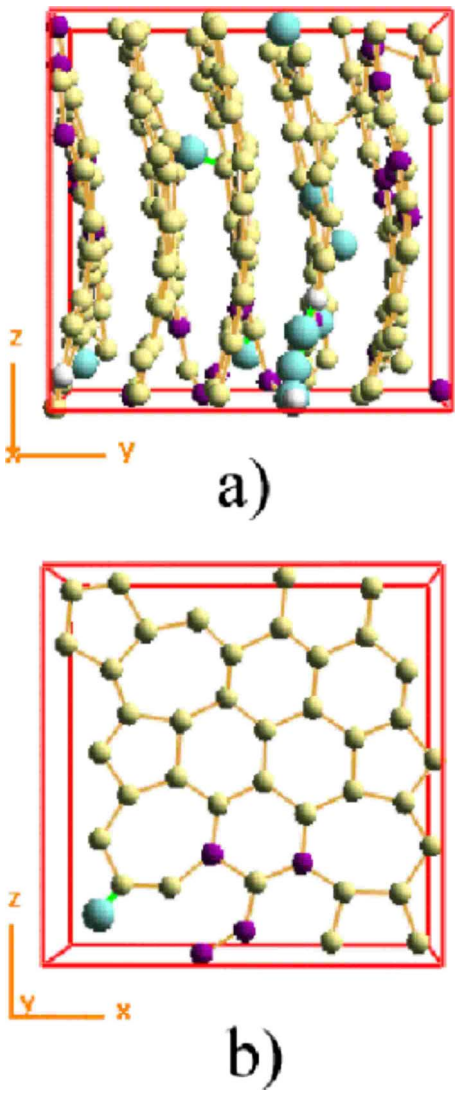

FIG. 9. (Color online) (a) A graphitic configuration containing ten hydrogen atoms generated at 3.9 g/cc with slow cooling rate. (b) A single damaged graphene sheet. Color coded as in Fig. 1.

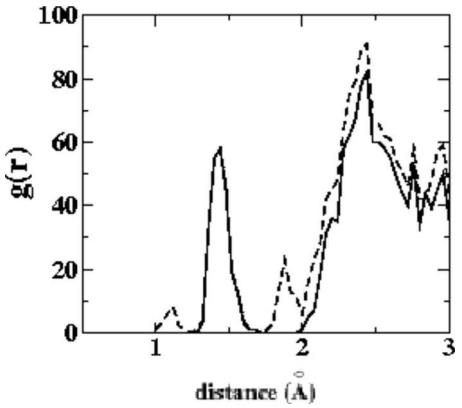

FIG. 10. Radial distribution function of hydrogenated graphite containing 25 hydrogen atoms generated at 3.9 g/cc with the slow cooling rate (dashed line) compared with the partial radial distribution function of C-C bonds only (solid line).

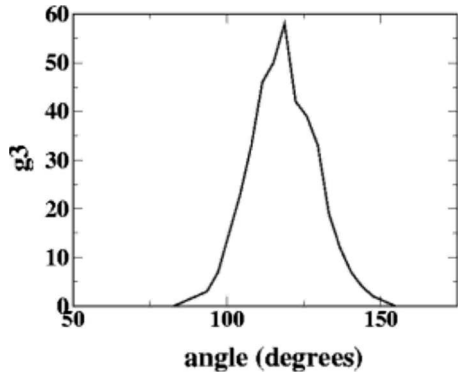

FIG. 11. Angular distribution function of hydrogenated graphite containing 25 hydrogen atoms generated at 3.9 g/cc with the slow cooling rate.

hydrogen content of the samples as well as the pressure (density) and cooling rates were varied. Most of the samples generated in this way contained ta-C:H, i.e., were mostly sp^3 bonded. The hydrogen atoms bonded mainly with carbon atoms that have three carbon neighbors. The number of carbon atoms with four carbon neighbors decreases as the hydrogen content increases, while the total number of sp^3-coordinated carbon atoms increases but was not a monotonic function of hydrogen concentration. The average length of the C-H bond was found to be 1.13 Å, which is slightly longer than the C-H distance in methane (1.09 Å). The increase in hydrogen content leads to a reduction in the band gap in our samples; the band gap disappeared for more than ten hydrogen atoms. This is due to the increase in the number of sp^2-bonded carbon atoms.

All the samples, whose final phase was amorphous, contained large pure sp^3 clusters from which the hydrogen atoms had been expelled. Some of these sp^3 clusters could be identified as nanodiamond crystallites. AViz (Ref. 17), which we used in this work, helped to identify the diamond clusters. The probability of precipitation of diamond crystallites in our simulations increases as the density is increased, and cooling rate increases independently of the hydrogen content. These trends are in qualitative agreement with experimental results of the bias-enhanced nucleation picture[6] and also with the trends observed in detonation diamond nucleation,[20] where increasing pressure (density) and faster cooling rates lead to a higher diamond fraction in the detonation soot. The diamond clusters generated inside hydrogenated amorphous carbon network are smaller and of poorer quality than those formed without hydrogen atoms in our previous paper.[15] This is in disagreement with the experimental results of Lifshitz *et al.*,[6] who argued that the probability of diamond nucleation in hydrogenated matrix is higher. However the conditions of our simulations (range of densities and hydrogen contents) differed from those in the experiments of Lifshitz *et al.*[6]

At slow cooling rates graphitic configurations appeared in both hydrogenated and pure carbon samples. The probability of formation of these graphitic configurations decreases as the cooling rate and density increase and is independent of hydrogen content. As explained in the experimental study of Titov *et al.*[20] during the cooling process, the system passes through a pressure-temperature region in the carbon phase diagram where the graphitic phase is preferable. Therefore as the time spent in this region increases (cooling rate decreases) the probability of the formation of graphite increases.

These are simulations of nucleation of nanodiamond and nanographite crystallites in the presence of hydrogen from a totally disordered compressed liquid phase. The results support the model of diamond nucleation induced by energetic species that was proposed by Lifshitz *et al.*,[6] where pure sp^3 clusters could precipitate in amorphous hydrogenated carbon formed on a substrate via a subplantation process and the experimental observation of nanographitic crystallites.[9]

ACKNOWLEDGMENTS

We are grateful to Y. Lifshitz and. A. Hoffman for useful discussions. We thank A. Horsfield and M. Finnis for providing us with the OXON package.

*phr76ja@techunix.technion.ac.il

[1] Hugh O. Pierson, *Handbook of Carbon, Graphite and Fullerenes* (Noyes, New Jersey, 1993).
[2] J. Robertson, Mater. Sci. Eng., R. **37**, 129 (2002).
[3] D. Saada, J. Adler, and R. Kalish, Phys. Rev. B **61**, 10711 (2000).
[4] C. E. Nebel and J. Ristein, *Thin Film Diamond I*, Semiconductor Science and Semimetals Vol. 76 (Elsevier, New York, 2003).
[5] D. P. Erchak, A. G. Ulyashin, R. B. Gelfand, N. M. Penina, A. M. Zaitsev, V. S. Varichenko, V. G. Efimov, and V. F. Stelmakh, Nucl. Instrum. Methods Phys. Res. B **69**, 271 (1992).
[6] Y. Lifshitz, Th. Kohler, Th. Frauenheim, I. Guzmann, A. Hoff-

man, R. Q. Zhang, X. T. Zhou, and S. T. Lee, Science **297**, 1531 (2002).
[7] Y. Lifshitz, X. M. Meng, S. T. Lee, R. Akhveldiany, and A. Hoffman, Phys. Rev. Lett. **93**, 056101 (2004).
[8] Sh. Michaelson and A. Hoffman, Diamond Relat. Mater. **14**, 470 (2005).
[9] E. H. T. Tao, B. K. Tang *et al.*, Adv. Mater. (Weinheim, Ger.) (to be published).
[10] G. Kopidakis, C. Z. Wang, C. M. Soukoulis, and K. M. Ho, Phys. Rev. B **58**, 14106 (1998).
[11] O. Ofer, J. Adler, and A. Hoffmann, Int. J. Mod. Phys. C **17**, 959 (2006).
[12] K. Kohary, S. Kugler, Z. Hajnal, T. Köhler, T. Frauenheim, S. Kátai, and P. Deák, Diamond Relat. Mater. **11**, 513 (2002).
[13] M. M. M. Bilek, D. R. McKenzie, D. G. McCulloch, and C. M. Goringe, Phys. Rev. B **62**, 3071 (2000).
[14] S. Iarlori, G. Galli, and O. Martini, Phys. Rev. B **49**, 7060 (1994).
[15] A. Sorkin, Joan Adler, and R. Kalish, Phys. Rev. B **74**, 064115 (2006).
[16] C. Z. Wang, K. M. Ho, and C. T. Chan, Phys. Rev. Lett. **70**, 611 (1993).
[17] J. Adler, A. Hashibon, N. Schreiber, A. Sorkin, S. Sorkin, and G. Wagner, Comput. Phys. Commun. **147**, 665 (2002).
[18] C. Z. Wang and K. M. Ho, Phys. Rev. Lett. **71**, 1184 (1993).
[19] A. P. Horsfield, Phys. Rev. B **56**, 6594 (1997).
[20] V. M. Titov, V. F. Anisichkin, and I. Yu. Mal'kov, Fiz. Goreniya Vzryva **25**, 117 (1989).